Structural analysis of water in ionic liquid domains – A low pressure study

Dziubinska-Kühn, Katarzyna; Croese, Jared; Pupier, Marion; Matysik, Jörg; Viger-Gravel, Jasmine; Karg, Béatrice; Kowalska, Magdalena

How to cite

DZIUBINSKA-KÜHN, Katarzyna et al. Structural analysis of water in ionic liquid domains – A low pressure study. In: Journal of Molecular Liquids, 2021, vol. 334, n° 116447. doi: 10.1016/j.molliq.2021.116447

This publication URL: https://archive-ouverte.unige.ch/unige:152389
Publication DOI: 10.1016/j.molliq.2021.116447

Journal of Molecular Liquids 334 (2021) 116447

Contents lists available at ScienceDirect

Journal of Molecular Liquids

journal homepage: www.elsevier.com/locate/molliq

Structural analysis of water in ionic liquid domains – A low pressure study

Katarzyna Dziubinska-Kühn [a,b], Jared Croese [a,c], Marion Pupier [d], Jörg Matysik [b], Jasmine Viger-Gravel [d], Beatrice Karg [a,c], Magdalena Kowalska [a,*]

[a] Experimental Physics Department, CERN, 1211 Geneva, Switzerland
[b] Institute of Analytical Chemistry, University of Leipzig, D-04103 Leipzig, Germany
[c] Department of Nuclear and Particle Physics, University of Geneva, 1211 Geneva, Switzerland
[d] Department of Organic Chemistry, University of Geneva, 1211 Geneva, Switzerland

ARTICLE INFO

Article history:
Received 11 February 2021
Revised 22 April 2021
Accepted 7 May 2021
Available online 14 May 2021

2000 MSC:
0000
1111

Keywords:
Ionic liquid
Water
Structural arrangement
Nuclear Magnetic Resonance
Vacuum

ABSTRACT

Imidazolium-based ionic liquids (ILs) are frequently used solvents, due to their peculiar structure resulting in low melting points. Recent studies revealed the direct impact of the water molecules on the self-structuring of the IL nano-domains. Therefore, in this work the influence of different water impurities on the IL network and its vacuum stability has been studied using Nuclear Magnetic Resonance (NMR) and Electrochemical Impedance Spectroscopy (EIS). As a result, three distinguishable interdependent regions could be identified. Degassing of solutions with different IL-H_2O ratios proved a strong dependence of the removed water species on the initial composition of the doped IL nano-domains. Consequently, selective purification of targeted cavities, based on vacuum extraction, is proposed as a novel tool to control the structural rearrangement of the ionic liquid networks in the presence of water.

1. Theoretical introduction

Since ionic liquids (ILs) were discovered in 1914[1], this class of compounds continuously attracts the attention of various fields in science[2–8]. The most basic definition of ILs describes them as molten salts, consisting entirely of ions. Because of their structural arrangement[9,10], they can easily encapsulate small molecules, such as short-chain alcohols or CO_2[11–13]. This ability, together with a low melting point and a low volatility, has turned ILs into one of the most studied industrial solvent family.

All the imidazolium-based ionic liquids demonstrate a similar structural arrangement, resulting from the presence of polar (aromatics rings coordinated by the anions trapped between them) and non-polar (between the aliphatic chains of the neighbouring cations) nano-domains[9,14,15]. This type of aggregation is additionally enhanced by the presence of π-π stacking between the aromatic rings[16,17]. The influence of the anions on the nano-domains depends on its size as well as the molecular shape, but stays independent of the length of the aliphatic chain in the cation[18]. Because anions are coordinated inside of the polar domains created by four (within the plane) or eight (between the planes) imidazolium rings, large and bulky ions, such as octanoate ($OOct^-$) or bis(trifluoromethanesulfonyl) imide (Tf_2N^-)[19], do not fit those cavities and therefore distort the periodic network of the IL[16,20,21]. The characteristic cation–anion network of C_n-MIM-based ILs results in their aprotic character, high thermal stability[22], always retaining high density[23] and high viscosity [24].

Because of its permanent dipole moment[25], the dicyanamide (DCA^-) anion is one of the most frequently used to design ILs with revised electrochemical applications[25,26]. Especially, 1-ethyl-3-methylimidazolium dicyanamide (EMIM-DCA) is known for ultra low viscosity and thus high conductivity in comparison with other EMIM-based liquids[25,4,27]. Additionally, its local packing was proven to be much more dense than other solvents from the imida-

* Corresponding author.
E-mail address: magdalena.kowalska@cern.ch (M. Kowalska).

https://doi.org/10.1016/j.molliq.2021.116447
0167-7322/

zolium solvents family[5]. EMIM-DCA is often used for tailor-made membranes for CO_2 separation or ionic jelly polymers[28,25], or serves as the solvent in extractive distillation of water-alcohol mixtures and even reaction media in biotechnology[29,30].

Nuclear Magnetic Resonance (NMR) spectroscopy is known as an excellent technique to study the structural and kinetic aspects of ILs. In 1994, Welton *et al.* used the sensitivity of the environment, chemical shift (CS), relation to study the interactions between the neighbouring $EMIM^+$ cations, driven by the presence of ring current effect[31]. The CS of the acidic proton H-2[18,32] is the most responsive to the changes in the local environment [33]. It facilitates the analysis of the cation–anion competition for hydrogen bonding with water molecules[34]. Consequently, the perturbation of CS upon titration serves perfectly to establish the critical micelle concentration (CMC) of the C_nMIM cations. The same information can be extracted from spin–lattice relaxation rates (R_1)[35], which, over a range of temperatures, are known to be a precise indicator for the thermal structural interconversion of the imidazolium-based ILs with a short side alkyl chain[20]. 2D NMR experiments, such as NOESY or ROESY, are frequently used to understand the structural arrangement of neat IL networks[36]. In addition, the presence of NOE kinetics[37] allows to predict the intermolecular distances between neighbouring cation and anion[38,39,16]. A different approach employs 2D DOSY experiments to determine the diffusion coefficients in neat ILs and IL-water mixtures[40,41].

The most important, but often neglected feature of the short side-chain $C_n$mim-ILs is their high hygroscopicity[42,43]. However, in the case of some ILs, water impurities can be removed with purification techniques based on ultra-high vacuum (UHV) degassing[44] or gas dehydration[45]. An interesting reversed approach employs intentional doping of the IL network with water molecules, in order to modify the overall properties, such as density or viscosity[46–48,11].

Multiple molecular dynamics (MD) studies confirmed the presence of single water molecules in ILs (frequently described as "free" molecules) and small water clusters in the mixtures with low water fraction $X_{H_2O} \leqslant 0.2$[49–51]. This type of water aggregation directly results from the binding affinity of the IL anion in the polar domains, due to the $EMIM^+$ cation being proven to be a weak proton donor[52]. The DCA^- anion can strongly attract water molecules and therefore control the existence and size of possible water aggregates[53–55]. If the water fraction is small, in the presence of a hydrophobic anion, it is expected to incorporate as single molecules preferring to form a hydrogen bond (HB) network in the mixed anion-water environment, rather than self-aggregate [50].

Various studies on the advantages of the doping of $C_n$mim-based solvents with small molecules have proven the direct impact of the presence of water on the electrochemical properties of the ionic liquids[56,57]. Multiple studies confirmed the differences in the nanosegregation of 1-alkyl-3-methylimidazolium based ILs in both, bulk and liquid–solid or liquid-vacuum interfaces[58,59]; governed by structure of cation, length of the side alkyl chain, and most importantly structure and size of anion[14,60–62]. However, despite extensive studies on the water behaviour during IL titration up to the water molar fraction X_{H_2O} = 0.990, the reversed mechanism of the removal of water molecules was not quite studied, yet. In this work, the influence of different vacuum regimes on the IL-water mixtures is analysed for several initial molar fractions of water. The applied degassing conditions allowed to restructure water molecules into clusters remaining stable inside of the selected domains in the short side-chain C_nMIM-based IL network. This occurrence of the selective purification of ionic liquids is opening the pathway to tailor-made water-IL mixtures.

2. Experimental

2.1. Materials

1-Ethyl-1-methylimidazolium dicyanamide and D_2O were purchased from Sigma–Aldrich with 98.5% and 99.9% purity, respectively. H_2O was deionized with a commercially available Milli-Q water purification system purchased from Merck. If not mentioned differently, IL was used without further purification. During the sample preparation (see Tab. S-1), H_2O was added to EMIM-DCA and stirred using vortex mixer for few seconds. Afterwards, D_2O was added to the IL-H_2O mixture and the solution was again stirred using vortex mixer for 1–2 min. All atmospheric pressure NMR measurements were conducted less than an hour from the sample preparation.

2.2. Methods

2.2.1. NMR

Spin–lattice relaxation time and standard 1D single pulse measurements were conducted using an Avance Neo 400 and Avance III 500 Spectrometers (Bruker BioSpin GmbH) with magnetic fields of 9.4 T and 11.7 T, respectively. Samples were transported to the NMR tubes with an outer diameter of 5 mm, containing a D_2O capillary used for the external lock. Spectra were referenced against the capillary HDO peak. T_1 experiments were performed using the Inversion Recovery sequence (180° - inversion time (τ_i) - 90°) with τ_i containing 26 delays varying from 0.01 s to 40 s. After sample preparation (see Tab. S-1), all solutions were left for 30 min to equilibrate. All measurements were conducted at 298 K; the temperature was controlled within ±1°C. All spectra were acquired and processed with Topspin 4.0.5 (Bruker BioSpin GmbH).

Fits for the critical aggregation concentration (CAC) via the method of continuous variation have been performed using the SciPy Orthogonal Distance Regression (ODR) package, which implements a non-linear Levenberg–Marquardt-type algorithm. A linear ODR was performed to the first and last 10 and 12 points of chemical shift and relaxation data, respectively[63]. This allowed taking into account both the error on the peak areas/intensities/T_1 relaxation value, as well as the preparatory error (estimated to be less than 2%). Subsequently, the Python Uncertainties package was used to propagate the errors on the fit results to the final value of the CAC[64].

2.2.2. Electrochemical Impedance Spectroscopy

Impedance measurements were conducted using a potentiostat PGSTAT302N (Metrohm Autolab) equipped with the frequency response analyzer FRA32M. Two cylindrical platinum electrodes were immersed in 1.5 ml volume polypropylen cell, modified to be sealed due to the high hygroscopicity of EMIM-DCA. Electrodes were rinsed with EtOH and dried at room temperature (RT) between the measurements. A frequency range of 1–10^6 Hz was selected, using ten logarithmic frequency steps per decade (61 data points in total). After sample preparation (see Tab. S-1), all solutions were left for 60–80 min to equilibrate. Impedance spectra were recorded using Nova 2.1.4 software (Metrohm Autolab).

During processing, impedance spectra were fitted using the equivalent electrical circuit R(RQ)[11]. Obtained resistance was recalculated into conductance. All measurements were performed in doublets within 6% error and fitted independently.

2.2.3. Degassing of the samples

Volume of the samples before degassing was up-scaled to cover for a possible loss of 100% of the water volume. Solutions listed in Table 1 were transported to the low pressure J. Young valve NMR

Table 1
Labeling pattern, molecular ratio and molar fractions of water in the solutions, before degassing in process- and high-vacuum conditions.

Label	No. H_2O/1 EMIM-DCA	$X_{H_2O+D_2O}$
A	3.0	0.749
B	4.5	0.817
C	7.5	0.882
D	20.0	0.952

tubes (Wilmad) containing a vacuum-tight D_2O capillary, similarly as during the atmospheric pressure measurements. Young tubes were connected with a home-built setup located within the ISOLDE facility at CERN, where different vacuum conditions could be achieved. Process-vacuum (10^{-2} mbar - 10^{-4} mbar) conditions were applied for 10 h and the minimal value of pressure (4.5×10^{-3} mbar) was reached after ~1 h for each sample. High-vacuum (10^{-5} mbar - 10^{-9} mbar) conditions were applied on the same samples after keeping them at 4.5×10^{-3} mbar for 24 h. The final pressure (5.8×10^{-5} mbar) was reached after ~2 h and the total degassing time in the high vacuum was 24 h for each sample.

3. Results and discussion

3.1. Atmospheric pressure NMR

3.1.1. Splitting of the water peak

$^1H_1$ NMR 1D spectra acquired during the titration of EMIM-DCA with a 50:50 mixture of H_2O and D_2O revealed the splitting of the water peak in the chemical-shift range between 3.5 and 4.15 ppm. Selected spectra ($0.049 \leqslant X_{H_2O+D_2O} \leqslant 0.498$) are presented in Fig. 2, for all see Fig. S-1. This is generally attributed to a slowed H/D exchange between H_2O and HDO species present in the solution. This type of water behaviour results from the presence of well separated polar and non-polar domains in short-chained ILs[40]. Additionally, Fig. 2 shows a comparison of the water peak in the $^1H_1$ spectra for the sample containing molar fractions of water: X_{H_2O} = 0.284 (orange) and mixed solution of X_{H_2O} = 0.142 and X_{D_2O} = 0.142 (blue). Chemical shift perturbation between the more shielded HDO (3.67 ppm) and less shielded H_2O (3.69 ppm) protons is 0.02 ppm and stays constant during the titration between $0.049 \leqslant X_{H_2O+D_2O} \leqslant 0.665$. Consequently, the IL network is preserved in the presence of two water species up to the molar fraction $X_{H_2O+D_2O}$ = 0.665. Additionally, this behaviour proves the ability of short side-chain $C_n$mim-ILs ($n \leqslant 4$) to encapsulate water molecules in polar and non-polar domains[65]. Due to the high affinity with the anion and H-2 in the imidazolium ring (Fig. 1), their preference will be higher for polar domains.[66,32].

The presence of nano-domains in EMIM-DCA can be additionally confirmed using the relative intensity of the water peak represented as the % fraction of the total H_2O-D_2O mixture intensity (see Fig. 3). A slow decrease can be observed until it reaches a minimum of 55% maximum intensity at $X_{H_2O+D_2O}$ = 0.554. For $X_{H_2O+D_2O}$ = 0.749, the intensity of the H_2O peak returns to 100%, implying that no nano-domains are present in the IL and its network is disrupted. Consequently, there are no spatial restrictions for the H/D exchange of water molecules and only one water species HDO is visible in the spectrum, indicated by singular water peak. Neat EMIM-DCA without additional purification has shown traces of water in ^1H NMR. No splitting of the water peak was observed in the presence of 1 μL D_2O (X_{D_2O} = 0.015). This behaviour shows that below $X_{H_2O+D_2O}$ = 0.049, the separation of water molecules is sufficient to exclude the exchange between H_2O and HDO.

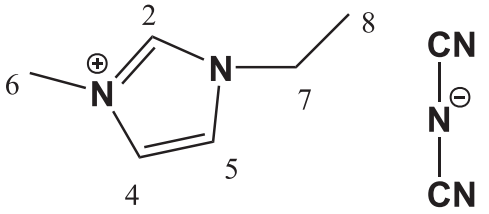

Fig. 1. The structure and labeling pattern of EMIM-DCA.

3.1.2. Chemical Shifts

The chemical shift difference ($\Delta\delta$) for $EMIM^+$ protons for $X_{H_2O+D_2O}$ changing from 0.049 to 0.990 is presented in Fig. 4. $\Delta\delta$ is calculated as the difference between the CS (δ) of the neat IL and the titrated sample ($\Delta\delta = \delta_{neat} - \delta_{sample}$) in ppm, selected for the clarity of the representation, because aromatic and aliphatic CS are in different regimes.

For $0.049 \leqslant X_{H_2O+D_2O} \leqslant 0.665$, where the IL network is preserved, all protons experience a systematic increase of $\Delta\delta$ due to the increasing number of water molecules stored in the polar and non-polar domains. Above $X_{H_2O+D_2O}$ = 0.907, only negligible changes of the chemical shifts (below 0.05 ppm) are observed upon the water addition. This indicates the presence of well-isolated cations and anions of EMIM-DCA, diluted with water molecules.

Between the occurrence of the nano-domains and saturated water solvation of the IL, a transition region can be seen. The chemical shifts of all protons increase more rapidly than before, during the titration from $X_{H_2O+D_2O}$ = 0.749 to $X_{H_2O+D_2O}$ = 0.882. This results from the disruption of the IL network and gradual degradation of the IL aggregates.

3.1.3. Critical Aggregation Concentration

If $n \leqslant 4$, the classical micelle formation of $C_n$mim-ILs is not observable[67] and the number of cations forming the higher order structure can not be clearly calculated[34]. However, a general critical aggregation concentration can be determined with the same method[68,69].

The method of continuous variation was employed to obtain CAC[70]. The average value estimated for the aromatic protons corresponds to the molar fraction $X_{H_2O+D_2O}$ = 0.832 (see Fig. 5). Average CAC value obtained for aliphatic protons (see Fig. S-2) is in good agreement with the aforementioned concentration. In addition, the CAC value estimated for water is similar to the results for the IL protons and equals $X_{H_2O+D_2O}$ = 0.832. This kind of agreement for the CAC illustrates the equal participation of all protons in the aggregation formation and thus, confirms its random character.

3.1.4. Spin–lattice relaxation

Measuring $^1H_1$ spin–lattice relaxation times (T_1) in the IL-water mixtures provides detailed information about the changes in the micro-environment and solvation patterns of the individual protons[35]. T_1 values for the protons in the neat EMIM-DCA (see Tab. S-2) are in good agreement with the relaxation times published for EMIM-BF_4 and EMIM-Tf_2N and vary by a factor of 1.3 (aromatic) and 1.4 (aliphatic) due to the change in the structure of the anion[71].

A systematic step-wise increase of the T_1 times is observed for all protons (see Tab. S-2). This behaviour of protons is directly linked to the larger number of water molecules present in the close neighbourhood of $EMIM^+$. The decrease of IL viscosity results in faster tumbling and therefore enhanced molecular motion, slowing down the relaxation[72].

The average CAC values obtained based on T_1 times correspond to the molar fraction $X_{H_2O+D_2O}$ = 0.882 for all protons, including

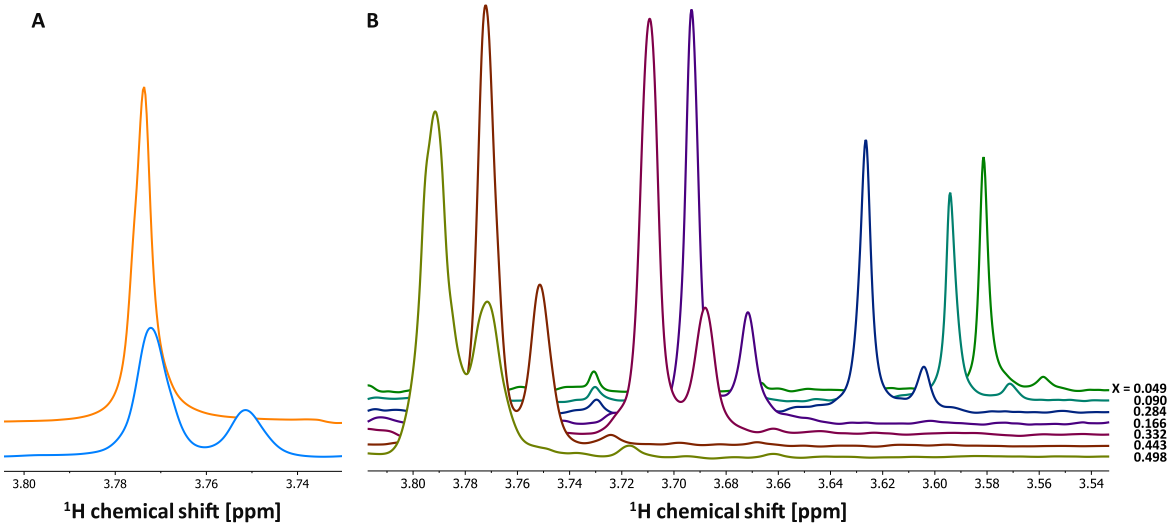

Fig. 2. ^{1}H NMR spectra of IL-water mixtures. **A**: Single water peak in the solution containing X_{H_2O} = 0.284 (orange) compared with the splitted H_2O/HDO peak in the solution containing mixed $X_{H_2O+D_2O}$ = 0.284. **B**: Gradual change of the CS and intensity of the H_2O and HDO peaks in the selected spectra between $0.049 \leqslant X_{H_2O+D_2O} \leqslant 0.498$. For all spectra showing the splitted water peak, see Fig. S-1.

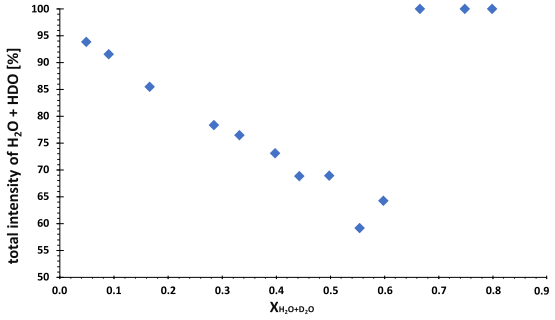

Fig. 3. Intensity of the H_2O peak shown as the % fraction of the total H_2O + HDO intensity, shown for solutions containing molar fraction of water $0.040 \leqslant X_{H_2O+D_2O} < 0.850$.

water molecules. T_1s presented in Fig. S-3 show a pattern confirming the presence of a CAC region with the previously determined transition region $0.665 < X_{H_2O+D_2O} \leqslant 0.907$.

Using an automated fitting procedure, errors of both methods can be determined yielding an uncertainty of 3% and 5%, for T_1 and chemical shift derived CAC, respectively. Thus, both methods exhibit comparable reliability to extract the CAC.

3.2. Electrical conductance

The conductance curve shown in Fig. 6 exhibits the presence of four regions, corresponding to the IL-H_2O regimes determined with ^{1}H NMR. Below $X_{H_2O+D_2O}$ = 0.665, a systematic increase of the conductance is observed due to the induced mobility of DCA^- anions upon the addition of water[73]. No extensive mobility of the cations is observed, because the IL network is preserved. Therefore, their participation in the overall conductance is considered to be constant. Following a maximum value of 37.8 mS for $0.665 < X_{H_2O+D_2O} < 0.749$, a steep decrease is observed up to $X_{H_2O+D_2O}$ = 0.832. This region has previously been associated with the breakdown of the IL nano-domains, followed by the systematic degrada-

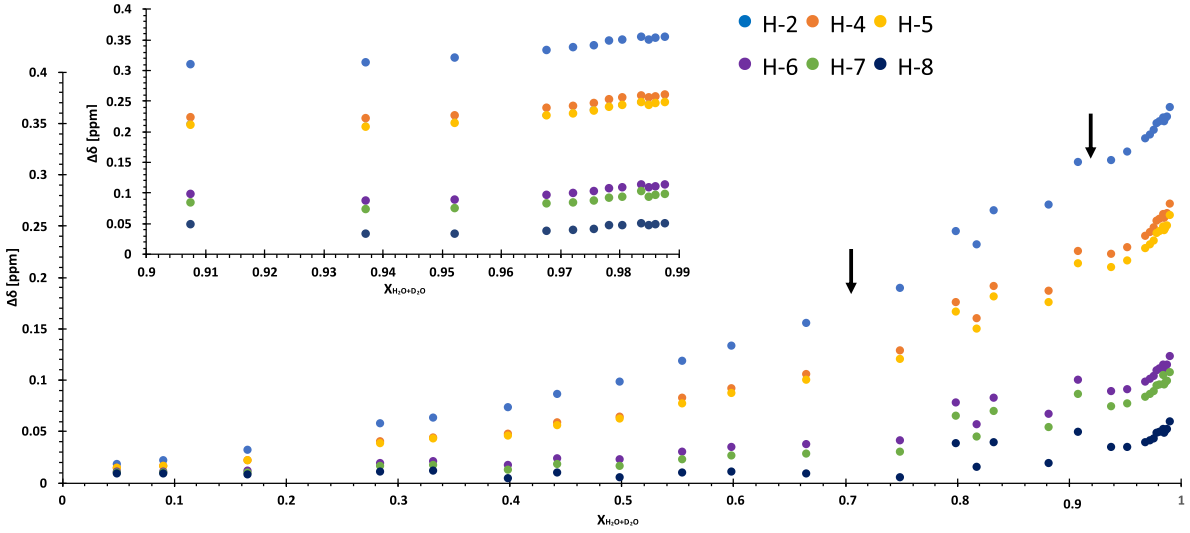

Fig. 4. The perturbation of chemical shift compared to neat IL $\Delta\delta$ for $EMIM^+$ protons, shown as a function of the molar fraction of water $X_{H_2O+D_2O}$. Black arrows (↓) indicate a changing point in the IL-H_2O regime.

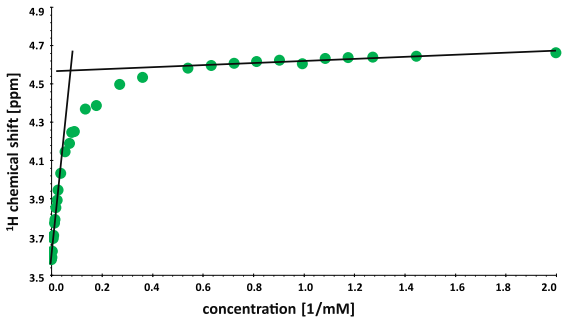

Fig. 5. Determination of the CAC using ^{1}H NMR CS of the water peak as a function of the reciprocal of water concentration. Linear least-squares fits were performed on the first and last 10 data points.

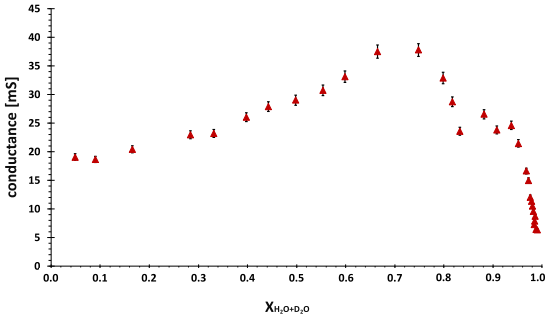

Fig. 6. Electrical conductance shown as a function of the molar fraction of water $X_{H_2O+D_2O}$.

tion of the IL-water aggregates. Here, the spontaneous interionic interactions will result in the significant reduction of the number of charge carriers due to the neutralization of IL cations and anions[74,75]. The CAC region is represented as the plateau between $0.832 < X_{H_2O+D_2O} \leqslant 0.907$[76,77]. For $X_{H_2O+D_2O} > 0.907$, a further steep decrease of conductance indicates the continued disruption of IL aggregates into smaller species diluted by the predominantly neutral water molecules[78].

3.3. Process vacuum NMR

Four solutions with $X_{H_2O+D_2O}$ values (see Table 1) representing the most dynamic IL-H_2O regimes were selected for degassing. **A**, **B** and **C** were chosen within both transition and CAC region. Solution **D** ($X_{H_2O+D_2O} = 0.952$) was selected above the CAC region. Therefore, both ionic liquid and water aggregations are expected to be present in the bicontinuous solution[51,49]. While the desorption process is mainly affecting the surface-near-area, it can also be influenced by the diffusion between different mixing states in bulk and liquid-vacuum interface[42,79]. Consequently, to achieve the interphase equilibrium, an extensive degassing time was provided and a waiting time of 5 h was additionally implemented between the vacuum application and NMR measurement. The excess of the solution allowed to detect the NMR signals only from the bulk liquid.

Analysis of the water content in the degassed samples is based on the comparison of the chemical shifts in **A** - **D** to the titrated solutions measured at atmospheric pressure. All ^{1}H 1D NMR results show good agreement for the aromatic proton chemical shifts (H-2, H-4 and H-5) and separately for the aliphatic protons (H-6, H-7 and H-8). In all spectra, before degassing no splitting of the water peak was observed and after degassing, it was present with $\Delta\delta = 0.02$ ppm between H_2O and HDO, proving that the polar and non-polar domains were fully reassembled in the IL network.

3.3.1. Polar and non-polar domains

Chemical shifts observed in **A** - **C** show a strong disproportion between the water occurrence in the polar and non-polar domains at atmospheric pressure and process-vacuum conditions. The CS of H-6, H-7 and H-8 stay in good agreement for **A**, **B** and **C** and indicate a final molar fraction of water $X_{H_2O+D_2O} \leqslant 0.049$, while **D** corresponds to a twice higher fraction $X_{H_2O+D_2O} = 0.090$.

In comparison, all aromatic protons in solutions **A** - **C** are associated with larger molar fractions of water. This confirms the preferential water storage in the polar domains[10]. Interestingly, the trend for retaining water in **A** - **C** is reversed in comparison with initial solution composition (Fig. 7). For example, the CS values of H-2, H-4 and H-5 in **A** correspond to $X_{H_2O+D_2O} = 0.166$, but in **B** and **C** to a lower fraction $X_{H_2O+D_2O} = 0.090$.

CS of aromatic protons in **D** indicate a similar water fraction as in **A**. Thus, even if larger water clusters or mixed-environment aggregates are formed in the solution (as expected for this regime), they will not withstand the spatial restrictions of the domains driving the restoration of the IL network. Only small clusters will remain in process-vacuum conditions. Consequently, the solute–solvent interactions, such as Coulombic interactions between the hydrophilic anion and water molecule likely serve as the dominating driving force of the limitations of the structural arrangement inside of the polar domains[54].

3.3.2. Water behaviour

The chemical shift analysis of the polar and non-polar domains' environment indicates the direct influence of the water presence on the aromatic and aliphatic protons of EMIM-DCA. In addition to this information, the CS of H_2O and HDO provide detailed insight into the nature of water species formed in the IL network (Fig. 7).

The reversed arrangement of the CS of H_2O reflects the higher molar fraction of water observed in the solution with less water added before the degassing. This behaviour is related to the number of isolated water molecules, which increases systematically with higher water fraction in the solution[80]. Additionally, the number of water/water HB is proven to systematically decrease with lower water fraction[81]. At the same time, water clusters present in the system during the systematic increase of water fraction remain constant in their size even up to $X_{H_2O+D_2O} = 0.700$[81] and stay dispersed[53], which is in good agreement with the EMIM-DCA network defragmentation determined at $X_{H_2O+D_2O} = 0.665$.

The aforementioned water CS trend in **A** - **C** is analogous to that of CS for H-2, H-4 and H-5. However, the determined molar fractions of water are larger for two solutions: $X_{H_2O+D_2O} = 0.284$ for **A** and $X_{H_2O+D_2O} = 0.166$ for **B**, but stable $X_{H_2O+D_2O} = 0.090$ for **C**. The difference between the IL protons and water indicates changes in the environment experienced by the proton in water molecules. Due to this clear divergence, water should be considered as a consolidated cluster instead of a random anion-water network containing single water molecules. Thus, although the high binding affinity of DCA^- will lead to the incorporation of the majority of water molecules into the cation–anion spatial arrangement in the polar domains, the small water clusters can withstand the vacuum conditions much easier, up to the point of becoming vacuum-resistant, while the free water molecules in the polar domains will be degassed.

In summary, degassing of water vapour from EMIM-DCA solution in the process-vacuum regime can only remove a restrained number of water molecules. Consequently, after the polar domains are saturated with small water clusters, water is accommodated in the non-polar domains.

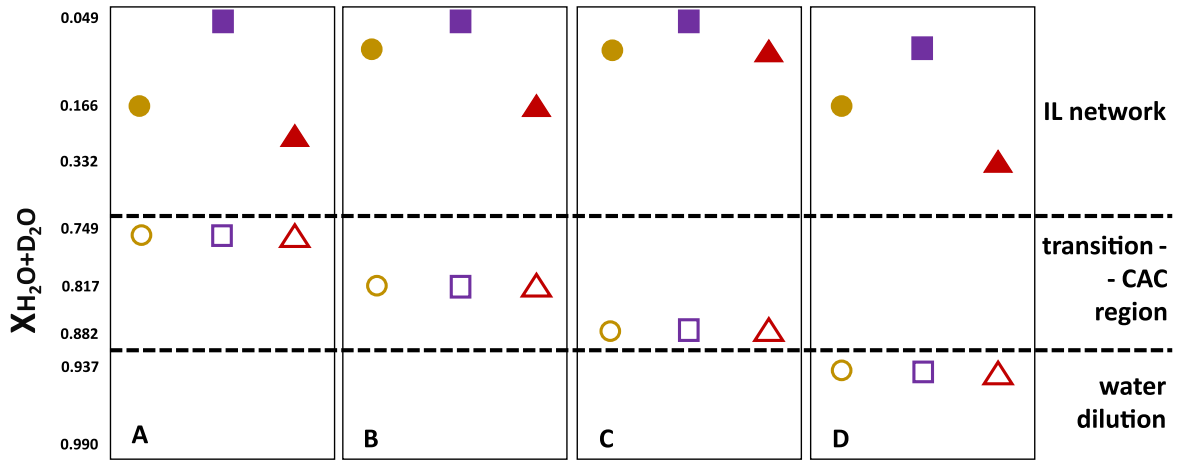

Fig. 7. Water molar fractions derived from the chemical shifts of EMIM-DCA and water in the solutions **A** - **D** (Table 1) at atmospheric pressure (hollow) and after degassing at process-vacuum conditions (solid). Molar fractions of water $X_{H_2O+D_2O}$ are shown as symbols: H-2, H-4 and H-5 (yellow dots); H-6, H-7 and H-8 (purple squares); H2O and HDO (red triangles) and assigned to the corresponding IL-water regions. The values of the water fractions on the y-axis were selected from among all studied fractions for clarity, for the exact values see table S-3.

3.4. High vacuum NMR

Contrary to the process-vacuum regime, the application of a high vacuum environment is a commonly used IL purification technique[82], if combined with high temperature[83].

Before the application of high vacuum conditions, **D** contained nearly seven times more water than **A** (accordingly 20.0 and 3.0 water molecules per 1 EMIM-DCA). After degassing, the CS of aromatic protons in both solutions can be attributed to the same molar fraction of water: $X_{H_2O+D_2O}$ = 0.284, whereas the storage capacity of polar domains was proven to be up to $X_{H_2O+D_2O}$ = 0.665. This behaviour confirms the absence of single water molecules in the degassed polar domains. Additionally, the CS of H_2O in sample **D** shows an excess of water ($0.332 < X_{H_2O+D_2O} < 0.398$) in comparison with the protons in the IL domains. Thus, water present in the ionic liquid network self-aggregates in a similar manner like in **A** - **C** and only small clusters are expected. However, it is important to mention that the nature of water molecules and/or their aggregates in the non-polar domains can not be deduced from the performed measurements.

Solutions **A**, **C** and **D** resulted equivalent CS for protons in the acquired ^{1}H spectra, corresponding to the trace amounts of water in pure EMIM-DCA (Fig. S-6). The analysed solutions were previously degassed in the process-vacuum regime, thus the high-vacuum conditions were applied on the selected water species built into the IL network. This indicates that only water clusters in the polar domains were able to disrupt the IL domains enough to overcome the binding affinities in the ionic liquid network. Therefore, more than one type of small water clusters is expected to exist in the process-vacuum regime, because the selective purification can happen only if different water molecules possess different binding energies, while the IL environment is limited and spatially restrained.

3.4.1. Splitting of the water peak

As mentioned before, EMIM-DCA containing negligible water impurities with small fraction of D_2O (X_{D_2O} = 0.015) added, did not reveal the presence of H/D exchange. This suggests a direct relation between the probability of the water-deuterium exchange and the number of water molecules trapped in the IL domains. If $X_{H_2O+D_2O}$ is too low, water molecules will not only not saturate all the cavities, but additionally will avoid the neighbouring cavities.

Table 2
Relative intensity of H_2O peak shown as the % fraction of the total water intensity (H_2O + HDO) in solutions degassed at process and high vacuum; The results for the degassed solutions are compared to the $X_{H_2O+D_2O}$ fractions for the non-degassed samples containing the same molar fraction of water (**atm equiv**).

	Process vacuum		High vacuum	
Label	% H_2O	atm equiv	% H_2O	atm equiv
A	57	79	57	no splitting
C	53	92	53	no splitting
D	52	73	54	no splitting

Such a behaviour has a direct influence on the water rearrangement in the process-vacuum solutions.

Two different water species have been observed independently in all the solutions in both vacuum regimes (see Fig. S-4 for process- and Fig. S-5 for high-vacuum regime). If compared with the intensity of H_2O and HDO peaks at atmospheric pressure conditions, a notable reduction is observed (Table 2). This suggests more than one water molecule present inside the domains is well isolated from other water molecules. Therefore, the H/D exchange does not happen between the domains (as proven for the non-degassed systems) but within the same cavity. However, this exchange is limited by the spatial constraints due to the molecular arrangement of water molecules inside a domain.

Additionally, no change in intensity ratios is observed for the H_2O-HDO peaks, when changing from process- to high-vacuum conditions. This indicates the removal of water in the larger clusters, present mainly in solutions **A** and **D**, and no influence on water dimers and monomers.

4. Summary and conclusions

In the present study, several independent regions were proven to exist during the titration of EMIM-DCA with a H_2O/D_2O mixture. Below $X_{H_2O+D_2O} \leqslant 0.665$, polar and non-polar domains dominate the structural arrangement of the IL network. Between $0.665 < X_{H_2O+D_2O} \leqslant 0.907$ a transition region exists, representing the extensive defragmentation of the IL aggregates. Within this range, a critical aggregation concentration was determined using ^{1}H chemical shifts (0.832 ± 0.025) and spin–lattice relaxation times (0.882 ± 0.044), both staying in good agreement. However, it should be emphasized that due to the random character of this process,

CAC indicates an aggregation region (herein confirmed between $0.832 < X_{H_2O+D_2O} \leqslant 0.907$) and not one specific molar fraction of water. For $X_{H_2O+D_2O} > 0.907$, the EMIM-DCA aggregates are systematically disrupted and diluted by the increased number of water molecules.

Degassing of the IL-water mixtures under process-vacuum conditions reveals a strong dependence of the polar and non-polar domains' saturation on the initial molar ratio between the two mixed solvents. Within the transition region, more water species present in the solution before degassing result in less water becoming vacuum-resistant in the polar domains, while non-polar domains are non-selectively purified. The chemical shift of water confirms the size of those species to be larger than single molecules.

When the vacuum conditions are applied on the solution with $X_{H_2O+D_2O}$ in the mutual solvation region, the IL network formed during degassing is confirmed to arrange around small water clusters in both polar and non-polar domains.

Under high-vacuum conditions, no selectivity is observed during purification and only traces of water can be confirmed in the analyzed solutions. However, no conclusion about the character of water species could be drawn.

The strong correlation between the process vacuum solution and its initial composition allows to consider degassing under process-vacuum conditions as a novel tool for selective ionic liquid purification. Doping of imidazolium-based ILs with small fractions of water is widely proven to improve their physicochemical properties, important especially for electrochemical applications. However, the structure–property relationship was so far only studied using theoretical approaches.

The presented experimental approach allows to remove selected water species from one type of IL nano-domains. This opens the pathway to possible control of the IL-water mixtures and their structural dependence on the type and location of water species in the IL network. Therefore, tailor-made degassed solutions balancing the intentional doping with water molecules and peculiar features of neat ILs can be easily customized.

Funding

This work has been sponsored by the Wolfgang Gentner Programme of the German Federal Ministry of Education and Research (Grant No. 05E15CHA), DFG Research Fellowship, European Research Council (Starting Grant No. 640465), CERN (Beta-DropNMR and gammaMRI MA Fund), and the Swiss Excellence Scholarship program.

Declaration of Competing Interest

The authors declare that they have no known competing financial interests or personal relationships that could have appeared to influence the work reported in this paper.

Acknowledgements

The authors would like to thank Tomasz Swebocki (University of Gdansk, Poland); Prof. Kaori Sugihara, Ewa Drab and Kristina Jajcevic (University of Geneva, Switzerland); Marianne Wenzel and Patrick Kurle (Leipzig University, Germany).

Appendix A. Supplementary material

Supplementary data associated with this article can be found, in the online version, at https://doi.org/10.1016/j.molliq.2021.116447.

References

[1] P. Walden, Molecular weights and electrical conductivity of several fused salts, Bull. Russian Acad. Sci (1914) 405–422.
[2] H. Zhao, H. Gao, G. Yu, Q. Li, Z. Lei, Capturing methanol and dimethoxymethane gases with ionic liquids, Fuel 241 (2019) 704–714, https://doi.org/10.1016/j.fuel.2018.12.010.
[3] X. He, H. Cheng, S. Yue, J. Ouyang, Quasi-solid state nanoparticle/(ionic liquid) gels with significantly high ionic thermoelectric properties, Journal of Materials Chemistry A 8 (2020) 10813–10821, https://doi.org/10.1039/d0ta04100a.
[4] T.J. Simons, P.C. Howlett, A.A. Torriero, D.R. MacFarlane, M. Forsyth, Electrochemical, transport, and spectroscopic properties of 1-ethyl-3-methylimidazolium ionic liquid electrolytes containing zinc dicyanamide, J. Phys. Chem. C 117 (2013) 2662–2669, https://doi.org/10.1021/jp311886h.
[5] T. Kobayashi, A. Kemna, M. Fyta, B. Braunschweig, J. Smiatek, Aqueous mixtures of room-temperature ionic liquids: Entropy-driven accumulation of water molecules at interfaces, J. Phys. Chem. C 123 (2019) 13795–13803, https://doi.org/10.1021/acs.jpcc.9b04098.
[6] M. Kar, O. Tutusaus, D.R. MacFarlane, R. Mohtadi, Novel and versatile room temperature ionic liquids for energy storage, Energy and Environmental Science 12 (2019) 566–571, https://doi.org/10.1039/c8ee02437e.
[7] G.A. Giffin, Ionic liquid-based electrolytes for beyond lithium battery technologies, Journal of Materials Chemistry A 4 (2016) 13378–13389, https://doi.org/10.1039/c6ta05260f.
[8] H. Qi, Y. Ren, S. Guo, Y. Wang, S. Li, Y. Hu, F. Yan, High-voltage resistant ionic liquids for lithium-ion batteries, ACS Applied Materials and Interfaces 12 (2020) 591–600, https://doi.org/10.1021/acsami.9b16786.
[9] J.N. Canongia Lopes, A.A. Pádua, Nanostructural organization in ionic liquids, Journal of Physical Chemistry B 110 (2006) 3330–3335. doi:10.1021/jp056006y.
[10] A. Mele, C.D. Tran, S.H. De Paoli Lacerda, The structure of a room-temperature ionic liquid with and without trace amounts of water: The role of C-H-O and C-H-F interactions in 1-n-butyl-3-methylimidazolium tetrafluoroborate, Angewandte Chemie - International Edition 42 (2003) 4364–4366, https://doi.org/10.1002/anie.200351783.
[11] R. Aranowski, I. Cichowska-Kopczyńska, B. Debski, P. Jasiński, Conductivity and viscosity changes of imidazolium ionic liquids induced by H_2O and CO_2, Journal of Molecular Liquids 221 (2016) 541–546, https://doi.org/10.1016/j.molliq.2016.06.010.
[12] S. Supasitmongkol, P. Styring, High CO_2solubility in ionic liquids and a tetraalkylammonium- based poly(ionic liquid), Energy and Environmental Science 3 (2010) 1961–1972, https://doi.org/10.1039/c0ee00293c.
[13] R. Babarao, S. Dai, D.E. Jiang, Understanding the high solubility of CO_2 in an ionic liquid with the tetracyanoborate anion, J. Phys. Chem. B 115 (2011) 9789–9794, https://doi.org/10.1021/jp205399r.
[14] K. Shimizu, M. Tariq, A.A. Freitas, A.A. Pádua, J.N. Lopes, Self-organization in ionic liquids: From bulk to interfaces and films, J. Braz. Chem. Soc. 27 (2016) 349–362, https://doi.org/10.5935/0103-5053.20150274.
[15] T. Niemann, D. Zaitsau, A. Strate, A. Villinger, R. Ludwig, Cationic clustering influences the phase behaviour of ionic liquids, Scientific Reports 8 (2018) 6–12, https://doi.org/10.1038/s41598-018-33176-6.
[16] A. Mele, G. Romanò, M. Giannone, E. Ragg, G. Fronza, G. Raos, V. Marcon, The local structure of ionic liquids: Cation-cation NOE interactions and internuclear distances in neat [BMIM][BF_4] and [BDMIM][BF_4], Angewandte Chemie - International Edition 45 (2006) 1123–1126, https://doi.org/10.1002/anie.200503745.
[17] R.P. Matthews, T. Welton, P.A. Hunt, Competitive π interactions and hydrogen bonding within imidazolium ionic liquids, PCCP 16 (2014) 3238–3253, https://doi.org/10.1039/c3cp54672a.
[18] P. Sanchora, D.K. Pandey, H.L. Kagdada, A. Materny, D.K. Singh, Impact of alkyl chain length and water on the structure and properties of 1-alkyl-3-methylimidazolium chloride ionic liquids, PCCP (2020) 17687–17704, https://doi.org/10.1039/d0cp01686a.
[19] K. Shimizu, C.E. Bernardes, J.N. Canongia Lopes, Structure and aggregation in the 1-alkyl-3-methylimidazolium Bis(trifluoromethylsulfonyl)imide ionic liquid homologous series, J. Phy. Chem. B 118 (2014) 567–576, https://doi.org/10.1021/jp409987d.
[20] S.M. Green, M.E. Ries, J. Moffat, T. Budtova, NMR and rheological study of anion size influence on the properties of two imidazolium-based ionic liquids, Scientific Reports 7 (2017) 1–12, https://doi.org/10.1038/s41598-017-09509-2.
[21] W. Levason, D. Pugh, G. Reid, Imidazolium-based ionic liquids with large weakly coordinating anions, New J. Chem. 41 (2017) 1677–1686, https://doi.org/10.1039/c6nj03674k.
[22] Y. Cao, T. Mu, Comprehensive investigation on the thermal stability of 66 ionic liquids by thermogravimetric analysis, Ind. Eng. Chem. Res. 53 (2014) 8651–8664, https://doi.org/10.1021/ie5009597.
[23] N.E. Cousens, L.J. Taylor Kearney, M.T. Clough, K.R. Lovelock, R.G. Palgrave, S. Perkin, Preparation and characterisation of high-density ionic liquids incorporating halobismuthate anions, Dalton Trans. 43 (2014) 10910–10919, https://doi.org/10.1039/c4dt00755g.
[24] M.C. Ribeiro, High viscosity of imidazolium ionic liquids with the hydrogen sulfate anion: A Raman spectroscopy study, J. Phys. Chem. B 116 (2012) 7281–7290, https://doi.org/10.1021/jp302091d.

[25] T. Carvalho, V. Augusto, Â. Rocha, N.M. Lourenço, N.T. Correia, S. Barreiros, P. Vidinha, E.J. Cabrita, M. Dionísio, Ion jelly conductive properties using dicyanamide-based ionic liquids, J. Phys. Chem. B 118 (2014) 9445–9459, https://doi.org/10.1021/jp502870q.
[26] L. Xu, X. Cui, Y. Zhang, T. Feng, R. Lin, X. Li, H. Jie, Measurement and correlation of electrical conductivity of ionic liquid [EMIM][DCA] in propylene carbonate and γ-butyrolactone, Electrochim. Acta 174 (2015) 900–907, https://doi.org/10.1016/j.electacta.2015.06.053.
[27] D.R. MacFarlane, J. Golding, S. Forsyth, M. Forsyth, G.B. Deacon, Low viscosity ionic liquids based on organic salts of the dicyanamide anion, Chem. Commun. 16 (2001) 1430–1431, https://doi.org/10.1039/b103064g.
[28] V.A. Kusuma, M.K. Macala, J. Liu, A.M. Marti, R.J. Hirsch, L.J. Hill, D. Hopkinson, Ionic liquid compatibility in polyethylene oxide/siloxane ion gel membranes, J. Membr. Sci. 545 (2018) 292–300, https://doi.org/10.1016/j.memsci.2017.09.086.
[29] E. Quijada-Maldonado, T.A. Aelmans, G.W. Meindersma, A.B. de Haan, Pilot plant validation of a rate-based extractive distillation model for water-ethanol separation with the ionic liquid [emim][DCA] as solvent, Chem. Eng. J. 223 (2013) 287–297, https://doi.org/10.1016/j.cej.2013.02.111.
[30] A.P. De Los Ríos, F.J. Hernández-Fernández, F.A. Martínez, M. Rubio, G. Víllora, The effect of ionic liquid media on activity, selectivity and stability of Candida antarctica lipase B in transesterification reactions, Biocatal. Biotransform. 25 (2007) 151–156, https://doi.org/10.1080/10242420701379213.
[31] A.G. Avent, P.A. Chaloner, M.P. Day, K.R. Seddon, T. Welton, Evidence for hydrogen bonding in solutions of 1-ethyl-3-methylimidazolium halides, and its implications for room-temperature halogenoaluminate(III) ionic liquids, Journal of the Chemical Society, Dalton Trans. (1994) 3405–3413, https://doi.org/10.1039/DT9940003405.
[32] J.M. Voss, B.M. Marsh, J. Zhou, E. Garand, Interaction between ionic liquid cation and water: infrared predissociation study of $[bmim]^+\cdot(H_2O)_n$ clusters, PCCP 18 (2016) 18905–18913, https://doi.org/10.1039/C6CP02730J.
[33] N. Dias, K. Shimizu, P. Morgado, E.J.M. Filipe, J.N.C. Lopes, Charge templates in aromatic plus ionic liquid systems revisited: NMR experiments and molecular dynamics simulations, doi:10.1021/jp503130y.
[34] T. Singh, A. Kumar, Aggregation behavior of ionic liquids in aqueous solutions: Effect of alkyl chain length, cations, and anions, J. Phys. Chem. B 111 (2007) 7843–7851, https://doi.org/10.1021/jp0726889.
[35] Y. Zhao, S. Gao, J. Wang, J. Tang, Aggregation of ionic liquids $[C_nmim]Br$ (n = 4, 6, 8, 10, 12) in D_2O: A NMR study, J. Phys. Chem. B 112 (2008) 2031–2039, https://doi.org/10.1021/jp076467e.
[36] R.A. Mantz, P.C. Trulove, R.T. Carlin, R.A. Osteryoung, ROESY NMR of basic ambient-temperature chloroaluminate ionic liquids, Inorg. Chem. 34 (1995) 3846–3847, https://doi.org/10.1021/ic00118a042.
[37] D. Braun, O. Steinhauser, The intermolecular NOE is strongly influenced by dynamics, PCCP 17 (2015) 8509–8517, https://doi.org/10.1039/c4cp04779f.
[38] Y. Lingscheid, S. Arenz, R. Giernoth, Heteronuclear NOE spectroscopy of ionic liquids, ChemPhysChem 13 (2012) 261–266, https://doi.org/10.1002/cphc.201100622.
[39] Y. Lingscheid, M. Paul, A. Bröhl, J.M. Neudörfl, R. Giernoth, Determination of inter-ionic and intra-ionic interactions in a monofluorinated imidazolium ionic liquid by a combination of X-ray crystallography and NOE NMR spectroscopy, Magn. Reson. Chem. 56 (2018) 80–85, https://doi.org/10.1002/mrc.4608.
[40] K. Saihara, Y. Yoshimura, S. Ohta, A. Shimizu, Properties of water confined in ionic liquids, Scientific Reports 5 (2015) 10619.
[41] V. Mazan, M. Boltoeva, Insight into the ionic interactions in neat ionic liquids by Diffusion Ordered Spectroscopy Nuclear Magnetic Resonance, J. Mol. Liq. 240 (2017) 74–79, https://doi.org/10.1016/j.molliq.2017.05.021.
[42] Y. Cao, Y. Chen, X. Sun, Z. Zhang, T. Mu, Water sorption in ionic liquids: Kinetics, mechanisms and hydrophilicity, PCCP 14 (2012) 12252–12262, https://doi.org/10.1039/c2cp41798g.
[43] C.D. Tran, S.H. De Paoli Lacerda, D. Oliveira, Absorption of water by room-temperature ionic liquids: Effect of anions on concentration and state of water, Appl. Spectrosc. 57 (2003) 152–157, https://doi.org/10.1366/000370203321535051.
[44] A. Taylor, K.R. Lovelock, A. Deyko, P. Licence, R.G. Jones, High vacuum distillation of ionic liquids and separation of ionic liquid mixtures, PCCP (2010) 1772–1783, https://doi.org/10.1039/b920931j.
[45] M. Krannich, F. Heym, A. Jess, Characterization of six hygroscopic ionic liquids with regard to their suitability for gas dehydration: density, viscosity, thermal and oxidative stability, vapor pressure, diffusion coefficient, and activity coefficient of water, J. Chem. Eng. Data 61 (2016) 1162–1176, https://doi.org/10.1021/acs.jced.5b00806.
[46] J.A. Widegren, E.M. Saurer, K.N. Marsh, J.W. Magee, Electrolytic conductivity of four imidazolium-based room-temperature ionic liquids and the effect of a water impurity, J. Chem. Thermodyn. 37 (2005) 569–575, https://doi.org/10.1016/j.jct.2005.04.009.
[47] J.A. Widegren, A. Laesecke, J.W. Magee, The effect of dissolved water on the viscosities of hydrophobic room-temperature ionic liquids, Chem. Commun. (2005) 1610–1612, https://doi.org/10.1039/b417348a.
[48] C.H.R. Carpio, L. King, R. Lindstrom, J. Nardi, Density and viscosity of several pure and water-saturated ionic liquids, Green Chem. 8 (2006) 172–180, https://doi.org/10.1039/B513231B.
[49] A. Sharma, P.K. Ghorai, Effect of water on structure and dynamics of [BMIM][PF_6] ionic liquid: An all-atom molecular dynamics simulation investigation, Journal of Chemical Physics 144 (2016), https://doi.org/10.1063/1.4944083.
[50] M. Moreno, F. Castiglione, A. Mele, C. Pasqui, G. Raos, Interaction of water with the model ionic liquid [bmim][BF_4]: Molecular dynamics simulations and comparison with NMR data, J. Phys. Chem. B 112 (2008) 7826–7836, https://doi.org/10.1021/jp800383g.
[51] C.E. Bernardes, M.E. Minas Da Piedade, J.N. Canongia Lopes, The structure of aqueous solutions of a hydrophilic ionic liquid: The full concentration range of 1-ethyl-3-methylimidazolium ethylsulfate and water, Journal of Physical Chemistry B 115 (2011) 2067–2074. doi:10.1021/jp1113202.
[52] M. Brehm, H. Weber, A.S. Pensado, A. Stark, B. Kirchner, Proton transfer and polarity changes in ionic liquid-water mixtures: A perspective on hydrogen bonds from ab initio molecular dynamics at the example of 1-ethyl-3-methylimidazolium acetate-water mixtures - Part 1, PCCP 14 (2012) 5030–5044, https://doi.org/10.1039/c2cp23983c.
[53] T. Méndez-Morales, J. Carrete, Ó. Cabeza, L.J. Gallego, L.M. Varela, Molecular dynamics simulation of the structure and dynamics of water-1-alkyl-3-methylimidazolium ionic liquid mixtures, J. Phys. Chem. B 115 (2011) 6995–7008, https://doi.org/10.1021/jp202692g.
[54] Y. Yasaka, C. Wakai, N. Matubayasi, M. Nakahara, Rotational dynamics of water and benzene controlled by anion field in ionic liquids: 1-butyl-3-methylimidazolium chloride and hexafluorophosphate, Journal of Chemical Physics 127. doi:10.1063/1.2768039.
[55] C. Schröder, T. Rudas, G. Neumayr, S. Benkner, O. Steinhauser, On the collective network of ionic liquid/water mixtures. I. Orientational structure, Journal of Chemical Physics 127. doi:10.1063/1.2805074.
[56] C. Zhao, A.M. Bond, R.G. Compton, A.M. O'mahony, E.I. Rogers, Modification and implications of changes in electrochemical responses encountered when undertaking deoxygenation in ionic liquids, Anal. Chem. 82 (2010) 3856–3861, https://doi.org/10.1021/ac100378g.
[57] A. Jarosik, S.R. Krajewski, A. Lewandowski, P. Radzimski, Conductivity of ionic liquids in mixtures, J. Mol. Liq. 123 (2006) 43–50, https://doi.org/10.1016/j.molliq.2005.06.001.
[58] D.W. Bruce, C.P. Cabry, J.N. Lopes, M.L. Costen, L. D'Andrea, I. Grillo, B.C. Marshall, K.G. McKendrick, T.K. Minton, S.M. Purcell, S. Rogers, J.M. Slattery, K. Shimizu, E. Smoll, M.A. Tesa-Serrate, Nanosegregation and structuring in the bulk and at the surface of ionic-liquid mixtures, J. Phys. Chem. B 121 (2017) 6002–6020, https://doi.org/10.1021/acs.jpcb.7b01654.
[59] J.L. Rivera, L. Molina-Rodríguez, M. Ramos-Estrada, P. Navarro-Santos, E. Lima, Interfacial properties of the ionic liquid [bmim][triflate] over a wide range of temperatures, RSC Advances 8 (2018) 10115–10123, https://doi.org/10.1039/c8ra00915e.
[60] M.H. Ghatee, A.R. Zolghadr, Surface tension measurements of imidazolium-based ionic liquids at liquid-vapor equilibrium, Fluid Phase Equilib. 263 (2008) 168–175, https://doi.org/10.1016/j.fluid.2007.10.004.
[61] J.R. Roscioli, D.J. Nesbitt, State-resolved scattering at room-temperature ionic liquid-vacuum interfaces: Anion dependence and the role of dynamic versus equilibrium effects, Journal of Physical Chemistry Letters 1 (2010) 674–678, https://doi.org/10.1021/jz900316g.
[62] K.B. Dhungana, L.F. Faria, B. Wu, M. Liang, M.C. Ribeiro, C.J. Margulis, E.W. Castner, Structure of cyano-anion ionic liquids: X-ray scattering and simulations, J. Chem. Phy. 145. doi:10.1063/1.4955186. https://doi.org/10.1063/1.4955186
[63] P.T. Boggs, J.E. Rogers, Statistical analysis of measurement error models and applications: proceedings of the AMS-IMS-SIAM joint summer research conference held June 10–16, 1989, in: Statistical analysis of measurement error models and applications: proceedings of the AMS-IMS-SIAM joint summer research conference held June 10–16, 1989, Vol. 112, Contemporary Mathematics, 1989, Ch. Orthogonal Distance Regression, p. 186. https://docs.scipy.org/doc/scipy-0.9.0/reference/odr.html.
[64] E.O. Legibot, Uncertainties: a python package for calculations with uncertainties. http://pythonhosted.org/uncertainties/.
[65] U. Schröder, J.D. Wadhawan, R.G. Compton, F. Marken, P.A. Suarez, C.S. Consorti, R.F. De Souza, J. Dupont, Water-induced accelerated ion diffusion: Voltammetric studies in 1-methyl-3-[2,6-(S)-dimethylocten-2-yl]imidazolium tetrafluoroborate, 1-butyl-3-methylimidazolium tetrafluoroborate and hexafluorophosphate ionic liquids, New J. Chem. 24 (2000) 1009–1015, https://doi.org/10.1039/b007172m.
[66] M. López-Pastor, M.J. Ayora-Cañada, M. Valcárcel, B. Lendl, Association of methanol and water in ionic liquids elucidated by infrared spectroscopy using two-dimensional correlation and multivariate curve resolution, Journal of Physical Chemistry B 110 (2006) 10896–10902. doi:10.1021/jp057398b.
[67] J.M. Vicent-Luna, J.M. Romero-Enrique, S. Calero, J.A. Anta, Micelle formation in aqueous solutions of room temperature ionic liquids: A molecular dynamics study, J. Phys. Chem. B 121 (2017) 8348–8358, https://doi.org/10.1021/acs.jpcb.7b05552.
[68] M. Blesic, H. Marques, N.V. Plechkova, K.R. Seddon, Self-aggregation of ionic liquids: micelle formation in aqueous solution (2007) 481–490. doi:10.1039/b615406a.
[69] V.A. Online, S. Cha, M. Ao, W. Sung, B. Moon, B. Ahlstro, P. Johansson, Y. Ouchi, D. Kim, Structures of ionic liquid – water mixtures investigated by IR and NMR spectroscopy (2014) 9591–9601. doi:10.1039/c4cp00589a.
[70] P. Job, Formation and stability of inorganic complexes in solution, Ann. Chim (1928) 113–203.
[71] R. Giernoth, D. Bankmann, N. Schlörer, High performance NMR in ionic liquids, Green Chem. 7 (2005) 279–282, https://doi.org/10.1039/b417783e.
[72] J.J. Allen, S.R. Bowser, K. Damodaran, Molecular interactions in the ionic liquid emim acetate and water binary mixtures probed via NMR spin relaxation and

exchange spectroscopy, PCCP 16 (2014) 8078–8085, https://doi.org/10.1039/c3cp55384a.
[73] J. Vila, P. Ginés, E. Rilo, O. Cabeza, L.M. Varela, Great increase of the electrical conductivity of ionic liquids in aqueous solutions, Fluid Phase Equilib. 247 (2006) 32–39, https://doi.org/10.1016/j.fluid.2006.05.028.
[74] A. Noda, K. Hayamizu, M. Watanabe, Pulsed-gradient spin-echo 1H and 19F NMR ionic diffusion coefficient, viscosity, and ionic conductivity of non-chloroaluminate room-temperature ionic liquids, J. Phys. Chem. B 105 (2001) 4603–4610, https://doi.org/10.1021/jp004132q.
[75] W.L. Yuan, X. Yang, L. He, Y. Xue, S. Qin, G.H. Tao, Viscosity, conductivity, and electrochemical property of dicyanamide ionic liquids, Frontiers in Chemistry 6 (2018) 1–12, https://doi.org/10.3389/fchem.2018.00059.
[76] R. Kamboj, P. Bharmoria, V. Chauhan, G. Singh, A. Kumar, S. Singh, T.S. Kang, Effect of cationic head group on micellization behavior of new amide-functionalized surface active ionic liquids, PCCP 16 (2014) 26040–26050, https://doi.org/10.1039/C4CP04054F.
[77] A. Boruń, Conductance and ionic association of selected imidazolium ionic liquids in various solvents: A review, J. Mol. Liq. 276 (2019) 214–224, https://doi.org/10.1016/j.molliq.2018.11.140.
[78] Z. Wojnarowska, E. Thoms, B. Blanchard, S.N. Tripathy, P. Goodrich, J. Jacquemin, J. Knapik-Kowalczuk, M. Paluch, How is charge transport different in ionic liquids? the effect of high pressure, PCCP 19 (2017) 14141–14147, https://doi.org/10.1039/c6cp08592j.
[79] H. Abe, T. Mori, R. Abematsu, Y. Yoshimura, N. Hatano, Y. Imai, H. Kishimura, Desorption process in room temperature ionic liquid based-mixtures under vacuum, J. Mol. Liq. 167 (2012) 40–46, https://doi.org/10.1016/j.molliq.2011.12.009.
[80] R. Macchieraldo, L. Esser, R. Elfgen, P. Voepel, S. Zahn, B.M. Smarsly, B. Kirchner, Hydrophilic ionic liquid mixtures of weakly and strongly coordinating anions with and without water, ACS Omega 3 (2018) 8567–8582, https://doi.org/10.1021/acsomega.8b00995.
[81] A.A. Niazi, B.D. Rabideau, A.E. Ismail, Effects of water concentration on the structural and diffusion properties of imidazolium-based ionic liquid-water mixtures, J. Phys. Chem. B 117 (2013) 1378–1388, https://doi.org/10.1021/jp3080496.
[82] A.W. Taylor, K.R.J. Lovelock, A. Deyko, P. Licence, R.G. Jones, High vacuum distillation of ionic liquids and separation of ionic liquid mixtures, PCCP 12 (2010) 1772, https://doi.org/10.1039/b920931j.
[83] S. Horike, M. Ayano, M. Tsuno, T. Fukushima, Y. Koshiba, M. Misaki, K. Ishida, Thermodynamics of ionic liquid evaporation under vacuum, PCCP 20 (2018) 21262–21268, https://doi.org/10.1039/c8cp02233j.